Terrain-inclination-based Three-dimensional Localization for Mobile Robots in Outdoor Environments

Xiaorui Zhu and Chunxin Qiu
State Key Laboratory of Robotics and System (HIT), Harbin Institute of Technology Shenzhen Graduate School, Shenzhen, Guangdong 518055, China
e-mail: xiaoruizhu@hitsz.edu.cn, qiu_chun_xin@163.com
Mark A. Minor
Department of Mechanical Engineering, University of Utah, Salt Lake City, Utah 84112
e-mail: minor@utah.edu

Received 23 April 2013; accepted 30 January 2014

A new terrain-inclination-based localization technique is proposed in this paper to enable a robot to identify its three-dimensional location relative to measurable terrain inclinations. Given a topographical map and a planned path, a robot-terrain-inclination model (RTI model) is extracted along the path on the terrain upon which the robot is operating. A particle filter is then used to fuse the measurement data with the robot motion based on the extracted RTI model for either a three-wheeled or a four-wheeled mobile robot. Experiments were carried out in four outdoor scenarios: one short path with different initial conditions and map resolution, another short path with different surface roughness and sensor accuracy, and two long paths with different types of rigid terrains and multiple loops. Experimental results show that the proposed method could achieve good localization performance on inclined outdoor terrains.

1. INTRODUCTION

In many outdoor environments, traditional sensors are used to achieve localization, such as laser range sensors, vision sensors, and sonar. But they need to detect physical landmarks to facilitate their localization, which does not work well for some outdoor situations. GPS is another popular tool for localization, but accuracy is limited and many environments block signals and preclude its application. Therefore, the goal of this research is to provide an alternative method of localization in three-dimensional space when GPS is low or lost for a period of time and the above traditional sensors are not suitable.

In this paper, a new terrain-inclination-based three-dimensional (3D) localization technique is developed for mobile robots operating on uneven terrain. The hypothesis is that the robots can localize themselves relative to a terrain characteristic map, such as a topographical map, as they travel over the uneven terrain. This new method is similar to how a human hiker or driver would localize himself (herself) along a trail by recognizing the terrain characteristics of particular trail segments, such as terrain inclination, surface type, traction capability, etc. While it is believed that both terrain inclination and surface type can be used to identify the position of the robot, only terrain-inclination information is applied here to prove the hypothesis. Using this technique, localization can be performed physically with limited onboard inertial sensors. Thus the information extracted from a known topographical map is combined with the motion model of the robot to achieve the robot localization.

In general outdoor situations, a robot moves on 3D inclined terrain [Figure 1(a)] while its topographical map is known *a priori* [see, for example, Figure 1(b)]. It is assumed that a specific path is planned on the above topographical map beforehand since this paper does not deal with motion-planning problems. It is clear that the robot's attitude would be varying when it is moving on the 3D inclined terrain. This phenomenon will be utilized in this paper to facilitate localization.

Therefore, the preplanned path (dashed line) on the topographical map of this navigation area is segmented into a series of quadrangles (dotted lines) that will be used to correlate with the robot plane when the robot moves; see Figure 2. The coordinate information of these quadrangles can be obtained from the given topographical map. According to the geometry, the robot-terrain inclination model (RTI model) can therefore be extracted for robot navigation. The RTI model is defined as describing the relationship between robot attitude (roll/pitch/yaw) and the position of the robot, where the roll and pitch vary according to the inclination changes of the natural terrain upon which the

Direct correspondence to: Xiaorui Zhu hit.zhu.xr@gmail.com

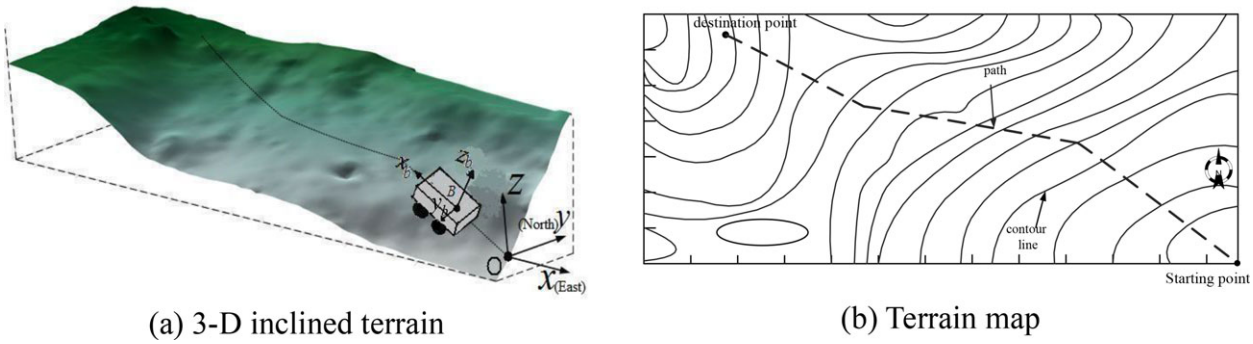

Figure 1. Outdoor scenario.

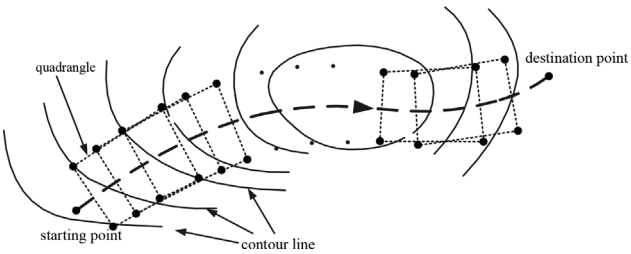

Figure 2. The projection of the robot motion plane on the topographical map.

robot is operating, and the yaw is determined once the path is given. Unlike traditional techniques in which physical landmarks define features on the map, terrain inclination is treated in this research as the primary environmental feature for outdoor mobile robots. The 3D inertial sensors are used here to measure the attitude and velocities of the robot, and a particle filter algorithm is used to incorporate the inertial sensor data to determine the 3D position of the robot based on the extracted RTI model.

The main contribution of this research involves a terrain-inclination-based localization technique to allow the robot to identify its three-dimensional position relative to a terrain characteristic map. An extraction algorithm is derived for the RTI model, and a particle filter algorithm is applied to achieve localization based on this model. Experiments then verify the terrain-inclination localization. The results demonstrate that a minimalist approach can be used to achieve localization on 3D inclined terrains. This terrain-inclination-localization technique serves as a fundamental basis for extension to more general outdoor environments, especially when GPS is lost.

The structure of this paper is as follows. Background on the current literature is discussed in Section 2. The particle filter terrain inclination 3D localization technique is proposed in Section 3. Experimental results and discussion are presented in Section 4. Conclusions are given in Section 5.

2. RELATED WORK

Mobile robots have been increasingly used in applications such as search and rescue (Roberts, Corke, Cunningham, & Durrant-Whyte, 1998), and planetary exploration (Weisbin et al., 1999), where the robots are required to travel over uneven terrain. In recent years, many aspects of research on mobile robots operating in uneven terrain areas have been studied, such as rough terrain modeling (Iagnemma & Dubowsky, 2004; Nasrallah, Angeles, & Michalska, 2005), terrain characterization (Brooks & Iagnemma, 2005; Talukder et al., 2002), and motion planning and control (Iagnemma & Dubowsky, 2004; Minor, Albiston, & Schwensen, 2006; Zhu, Minor, & Park, 2006; Zhu, Kim, Merrell, & Minor, 2007). However, the effectiveness of motion control depends in part on the accuracy of mobile robot localization.

In the past few decades, significant investigation of mobile robot localization has been performed (Borenstein, Everett, & Feng, 1996; Madhavan & Durrant-Whyte, 2004; Thrun, Burgard, & Fox, 2005). The traditional work on localization required laser range finders (Brenneke, Wulf, & Wagner, 2003; Chand & Yuta, 2010; Goulden, 2009; Manandhar & Shibasaki, 2001; Nagatani, Ishida, Yamanaka, & Tanaka, 2003; Surmann, Nuchter, and Hertzberg, 2003; Zhuang, Wang, Wang, & Xu, 2005), vision systems (Barfoot, 2005; Blaer & Allen, 2002; Burschka & Hager, 2004; Chekhlov, Pupilli, Mayol, & Calway, 2007; Cumani, Denasi, Guiducci, & Quaglia, 2003; Kawewong, Tongprasit, Tangruamsub, & Hasegawa, 2010), and sonar (Diosi & Kleeman, 2004; Laanaya, Martin, Khenchaf, & Aboutajdine, 2005). These sensors were used to measure the relative distance between the robots and some static or dynamic landmarks or features. Taking advantage of these sensors, most research in indoor environments has successfully achieved robot localization by detecting artificial landmarks or objects with sharp features, such as walls, corners, etc. (Burschka & Hager, 2004; Chekhlov et al., 2007; Cumani et al., 2003; Diosi & Kleeman, 2004; Surmann, Nuchter, and Hertzberg, 2003; Zhuang, Wang, Wang, & Xu, 2005). However, this has become much more challenging in outdoor environments

because of higher-dimensional terrains and the difficulties in detecting efficiently the features in a natural setting.

In the past few years, some researchers have started to focus on robot localization in outdoor environments (Barfoot, 2005; Blaer & Allen, 2002; Bonnifait, Bouron, Crubille, & Meizel, 2001; Bouvet & Garcia, 2000; Brenneke, Wulf, & Wagner, 2003; Chand & Yuta, 2010; Goulden, 2009; Kawewong et al., 2010; Laanaya et al., 2005; Manandhar & Shibasaki, 2001; Nagatani et al., 2003). A 3D laser range scanner (Brenneke, Wulf, & Wagner, 2003; Nagatani et al., 2003) was combined with a 2D simultaneous localization and mapping algorithm for autonomous navigation in an uneven environment. Manandhar and Shibasaki (2001) and Chand and Yuta (2010) used laser range finders to identify road crossings, buildings, and trees as different features for localization. While 3D laser range data are more informative in describing the features of the surroundings, real-time localization is easy to implement in the proposed method without the need for time-consuming data processing. The application of vision systems for localization has received increasing attention. Blaer and Allen (2002) utilized a color histogram to match omnidirectional images in order to topologically localize a mobile robot in urban outdoor environments. Their success rate was low, however, because the illumination in outdoor areas was highly dependent on the weather, or the time of day. To solve such a problem, various robust core algorithms have been developed for localization and mapping systems such as scale-invariant feature transform (SIFT) (Barfoot, 2005), the position-invariant robust feature (PIRF) (Kawewong et al., 2010), etc. But unpredictably long computation periods still caused the above techniques to fail for many real-time applications (Tongprasit, Kawewong, & Hasegawa, 2011). Laanaya et al. (2005) used sonar to identify landmarks such as huge rocks and cobbles, but sonar might not function well when landmarks are sparse. GPS is a popular solution to solve such outdoor localization problems (Bonnifait et al., 2001; Bouvet & Garcia, 2000). However, GPS signals might be inaccurate or even unavailable in some cases.

To tackle this problem, Lamon and Siegwart (2007) developed a special offroad rover with a passively articulated bogie and spring that could be combined with an inertial measurement unit (IMU) and wheel encoders to estimate the robot's pose. However, this method was only suitable for such a special mechanism. It is worth noting that terrain features have been used to achieve terrain following for military aircraft (Theunissen, Koeners, Rademaker, Jinkins, & Etherington, 2005; Zelenka, Clark, Zirkler, Saari, & Bragan, 1996), and bottom mapping/map matching (Cancilliere, 1994) has been used for underwater vehicles when GPS signals were lost. Resembling terrain following and bottom mapping/map matching, this research presents a new localization method in which the inclination characteristics of the terrain are considered as the features of the surroundings. Thus, this method can be applied to derive more accurate localization relative to a terrain map upon which the robot must navigate, and it provides supplemental localization when other traditional landmarks are unavailable, especially when GPS is blocked.

Various types of terrain maps have been used to represent outdoor environments. Topological maps are constructed to represent environments by nodes and edges. They can be scaled to large-scale environments, but they lack the ability to represent the geometric structure of an environment (Choset & Nagatani, 2001). Occupancy grid maps are another way to represent environments. The whole space is divided into a grid of cells that contain the occupancy evidence inferred from sensors (Martin & Moravec, 1996). Since the representation of the entire space must be stored in memory, even 2D evidence grids are large and expensive to copy. To reduce the processing and storage requirements, Fairfield, Kantor, and Wettergreen (2006) developed an octree data structure to implement an occupancy grid map for an underwater tunnel project. This type of map, however, would become expensive to copy when more particles are needed for accurate localization. Many authors used raw point clouds to represent a three-dimensional structure. However, the point cloud representation requires a higher computational load, although higher accuracy can be guaranteed (Brenneke, Wulf, & Wagner, 2003). To reduce the memory requirements, Hygounenc, Jung, Soueres, and Lacroix (2004) and Pfaff, Triebel, and Burgard (2007) used a standard elevation map (SEM) to represent the environment. The SEM consists of a two-dimensional grid in which each cell stores its elevation information. But vertical objects such as buildings and bridges are negligible in these maps, which would increase the difficulty of path planning. To overcome this problem, a multilevel surface (MLS) map can describe the environment in detail, but building such a map is more time-consuming because it consists of a two-dimensional grid in which each cell stores many surface patches that are represented by the mean and the variance of each measured height (Triebel, Pfaff, & Burgard, 2006). In this paper, a topographical map is utilized as the prior available terrain map for localization. The topographical map is characterized by contour lines and other graphical representations to portray natural and manmade features in outdoor environments. On such a map, vertical objects can be considered during motion planning, and less memory is used during navigation.

Recently, a few research groups, including the authors of this paper, began to take advantage of terrain maps for facilitating localization of mobile robots in outdoor environments (Kummerle, Triebel, Pfaff, & Burgard, 2008; Mandel & Laue, 2010). Kummerle et al. (2008) proposed a Monte Carlo localization of mobile robots in an outdoor environment relative to the MLS maps. The experiments predicted that this type of terrain map could facilitate outdoor localization without GPS signals. Mandel and Laue (2010) proposed a novel approach to take advantage of the road network

structure and its height profile on the SEM for position estimation when GPS is lost. Google's self-driving car also included a road network called RNDF (route network definition file) to be matched with the lane markers extracted from multiple laser sensors to increase the accuracy of localization (available at http://spectrum.ieee.org/). Fortunately, the above methods and the proposed technique in this paper are similar in spirit in that they all use basic terrain information to achieve localization. However, the method proposed in this paper focuses on facilitating autonomous navigation in 3D inclined outdoor terrains with only onboard inertial sensors to reduce the computational load of the algorithms instead of utilizing laser range sensors. Rather than being relative to the SEM or MLS maps, the terrain information is relative to a topographical map of the surrounding area that is measured offline by a motion capture system or is provided by other commercially available resources (available at http://www.bluewatersolutions.ca/lidar).

A new localization and mapping technique was recently published by our research group in which a preliminary version of the proposed localization method was incorporated (Zhu, Qiu, & Minor, 2013). This paper presents a comprehensive particle-filter-based 3D localization method using terrain inclination that was validated experimentally outdoors.

3. THREE-DIMENSIONAL TERRAIN-INCLINATION LOCALIZATION

3.1. Robot-terrain-inclination Model Extraction

Two frames are defined here: the inertial frame and the body frame. The inertial frame O is fixed to the earth-surface ellipsoid at the estimated initial position of the robot with three orthogonal axes (x, y, z) [see Figure 1(a)]. The y axis always points to the north pole of the earth, and the z axis points upward away from the earth's center. The body frame B is fixed to the midpoint of the rear axis of the robot with three orthogonal axes (x_b, y_b, z_b) [see Figure 1(a)]. The x_b axis is always consistent with the direction of the robot velocity, while the z_b axis is vertical to the robot plane. The robot path is represented by the trajectory of the origin in the body frame B. Roll, pitch, and yaw are determined with respect to x_b, y_b, and z_b, respectively. It is assumed that the mobile robot could be treated as a plane if the robot height is negligible relative to the scale of its travel distance, and that the traversing terrain is rigid.

Notice that the plane of the topographical map is the same as the x-O-y plane of the inertial frame. Assume that a preplanned path ($E'_1F'_1, \ldots, E'_jF'_j$) is given on the topographical map, which is the projection of the actual robot terrain path ($E_1\ F_1, \ldots, E_j\ F_j$) onto the x-O-y plane [see Figure 3(a)]. The path on the x-O-y plane is first segmented into a series of line segments with a fixed interval L_l/k, where L_l is the length of the robot and $E'_jF'_j$ represents the $j$thline segment [see Figure 3(a)]. A series of rectangles on the x-O-y plane, such as $A'_jB'_jC'_jD'_j$, can be plotted according to the geometrical relationship where L_w is the width of the robot. The points A'_j, B'_j, C'_j, D'_j, E'_j, and F'_j are the projections of the terrain points A_j,B_j,C_j,D_j,E_j, and F_j, respectively. The z value of these terrain points can be obtained by a weighted average interpolation method "Inverse Distance to a Power" from the topographical map (Chen, Li, & Ding, 2007). When the four-wheeled robot moves on the inclined 3D terrain, not all four wheels will touch the terrain. The center of gravity (CG) of the robot would help analyze the ground contact points once the robot platforms are confirmed. If the CG is located at the center of the robot, three terrain points among A_j,B_j,C_j,D_j with larger z components will be treated as the ground contact points. In this paper, the CG of our platform is close to the rear axis, so the rear wheels of the robot are assumed to always touch the ground. One of the front wheels might touch the ground while the other one would be suspended. When the robot moves above the jth quadrangle $A'_jB'_jC'_jD'_j$ along the path on the topographical map, the terrain points B_j and C_j represent the ground contact points of two rear wheels. Once another ground contact point (A_j or D_j) is determined, the robot plane at that moment will be obtained. Compare the z values of the terrain points A_j and D_j. If $z_{A_j} > z_{D_j}$, the left front wheel of the robot will touch the terrain point A_j and the right front wheel will be suspended. In this case, A_j will be the ground contact point, and the triangle $A_jB_jC_j$ will be used to represent the robot plane [see Figure 3(b)]. If $z_{D_j} > z_{A_j}$, then the right front wheel of the robot will touch the terrain point D_j and the triangle $B_jC_jD_j$ will be used to represent the robot plane at this moment [see Figure 3(b)]. When the three-wheeled robot moves on the 3D terrain, all three wheels will touch the terrain at the ground points B_j, C_j, and F_j, where $B_j$and C_j represent the ground contact points of two rear wheels, respectively, and F_j represents the ground contact points of the front wheel. Hence the triangle $B_jC_jF_j$ will be used to represent the robot plane in the case of the three-wheeled robot [see Figure 3(c)].

Once the robot plane is obtained, the next step is to extract the RTI model. In this section, a four-wheeled robot is used as the example for extraction of the RTI model. Suppose the triangle $B_j\ C_j\ D_j$ represents the robot plane and the $\overrightarrow{C_jD_j}$ represents the direction of the robot motion [see Figure 3(d)]. Notice that the origin of the body frame of the robot is coincident with the midpoint, O_j, of the terrain points B_j and C_j if the robot height is negligible. So the coordinates of O_j will be treated as the position of the robot. The coordinates of the points B_j,C_j, D_j, and O_j relative to the inertial frame are represented as (x_B, y_B, z_B), (x_C, y_C, z_C), (x_D, y_D, z_D), and (x_j, y_j, z_j), respectively. Then a robot-terrain-inclination model, RTI model : $(x_j, y_j, z_j) \rightarrow \gamma_M$ for the jth quadrangle, will be derived as a correlation function between the system states and the measurements for the particle filter presented later. In this model,

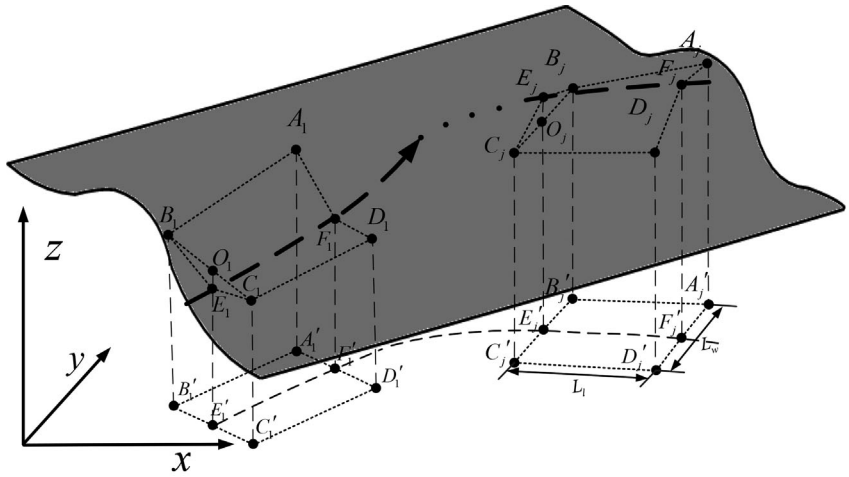

(a) The path on the *x*-*O*-*y* plane is segmented into a series of quadrangles.

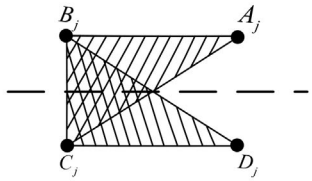

(b) Four-wheeled robot

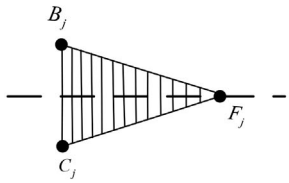

(c) Three-wheeled robot

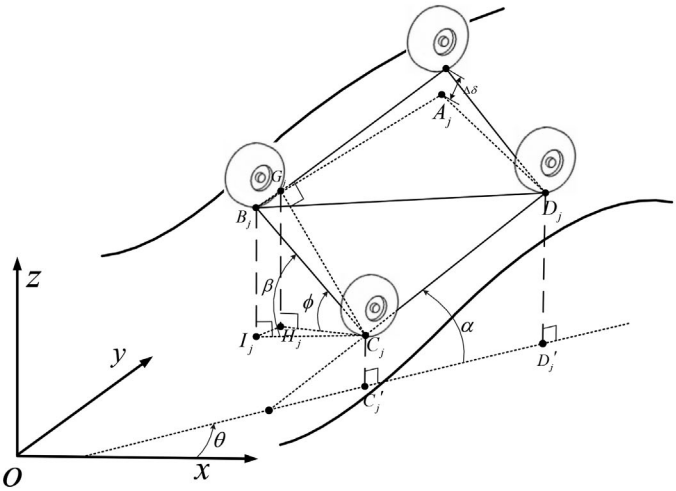

(d) Geometric extraction ($\Delta\delta$ represents the distance between the off-land wheel and the terrain point A_j).

Figure 3. Geometric extraction of the robot-terrain-inclination model.

$\gamma_M = [\theta_j \quad \alpha_j \quad \phi_j]^T$ represent the orientation angles of the robot plane according to the terrain information on the topographical map. These angles ϕ_j, α_j, and θ_j will be directly related to the roll, pitch, and yaw angles of the robot, respectively.

The heading angle, θ_j, is defined as the angle between the $\overrightarrow{C_j'D_j'}$ and the x axis. The heading angle is exclusively determined by the path. The angle α_j is defined as the one between the robot direction $\overrightarrow{C_jD_j}$ and the *x*-*O*-*y* plane. The plane $H_jI_jC_j$ is parallel to the *x*-*O*-*y* plane. β_j is the angle between the line $\overrightarrow{C_jI_j}$and $\overrightarrow{C_jB_j}$. ϕ_j is the angle between the $\overrightarrow{C_jB_j}$and the line $\overrightarrow{C_jH_j}$ [Figure 3(d)]. Then the angles $\alpha_j$and ϕ_j can be obtained from the following equations:

$$\alpha_j = \sin^{-1}\left(\frac{(z_D - z_C)}{\left|\overrightarrow{C_jD_j}\right|}\right), \tag{1}$$

$$\phi_j = \sin^{-1}\left(\frac{\sin\beta_j}{\cos\alpha_j}\right), \tag{2}$$

$$\beta_j = \sin^{-1}\left(\frac{(z_B - z_C)}{\left|\overrightarrow{B_jC_j}\right|}\right), \tag{3}$$

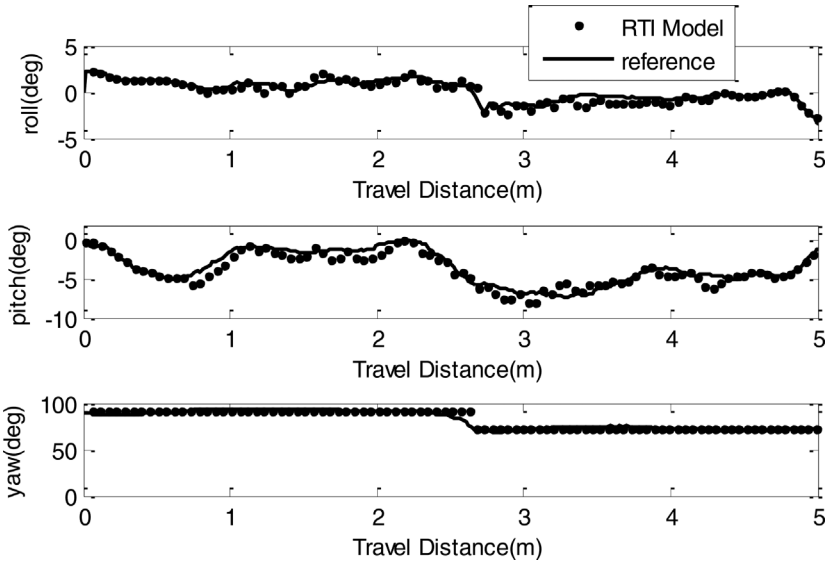

Figure 4. Verification of RTI model extraction.

$$\left|\overrightarrow{C_j D_j}\right| = \sqrt{(x_C - x_D)^2 + (y_C - y_D)^2 + (z_C - z_D)^2}, \tag{4}$$

$$\left|\overrightarrow{B_j C_j}\right| = \sqrt{(x_B - x_C)^2 + (y_B - y_C)^2 + (z_B - z_C)^2}. \tag{5}$$

Therefore, a number of angles $(\theta_j, \alpha_j, \phi_j)$ can be extracted from the serial quadrangles $A'_j B'_j C'_j D'_j$ [see Figure 3(a)]. Then the robot position (x_j, y_j, z_j) at each quadrangle corresponds with each group $(\theta_j, \alpha_j, \phi_j)$. By linear interpolation of the above discrete relationship, $[\theta_k \quad \alpha_k \quad \phi_k]^T =$ RTI model(x_k, y_k, z_k) can be obtained, $k = 1, 2, \ldots, N$. The number N can be adjusted for accuracy. Hence we finally get a series of discrete relationships between the robot attitude and the robot position.

To validate the above extraction algorithm of the RTI model, a simple experiment was carried out when the robot moved on the 3D inclined terrains at a speed of 0.2 m/s. The robot attitude calculated from the RTI model was compared with the reference one measured from a high-accuracy inertial measurement unit (NAV440 from Crossbow Technology®) (see Figure 4). Figure 4 indicates that the RTI model is effective in estimating the robot attitude with reasonable uncertainty. The similarity will be used later as a quantitative index of the uncertainty between the estimated attitude and the measured one. As the similarity decreases, the uncertainty increases. It is worth noting that the above derivation is based on a rigid wheeled robot. The vehicle suspension would certainly introduce uncertainty into the method. These uncertainties will be considered in Section 3.2 when the particle filter is applied.

3.2. Particle Filter Terrain-inclination Localization

Assume that the robot follows a given path where the terrain surface inclinations are not always zeros and the robot can measure its attitude and velocities. The 3D robot position is defined as the system state, X_t, which will be estimated using a Monte Carlo approach (Dellaert, Fox, Burgard, & Thrun, 1999). The basic idea of the Monte Carlo approach is to estimate the state X_t by a weighted set of M particles. The state transition of a single particle m through motion is described as

$$X_t^{[m]} = \begin{bmatrix} x_t^{[m]} \\ y_t^{[m]} \\ z_t^{[m]} \end{bmatrix} = \begin{bmatrix} x_{t-1}^{[m]} \\ y_{t-1}^{[m]} \\ z_{t-1}^{[m]} \end{bmatrix} + T\mathbf{A} \begin{bmatrix} v_{x_b} \\ v_{y_b} \\ v_{z_b} \end{bmatrix}, \tag{6}$$

where

$$\mathbf{A} = \begin{bmatrix} c\theta c\alpha & -c\theta s\alpha s\phi - s\theta c\phi & -c\theta s\alpha c\phi + s\theta c\phi \\ s\theta c\alpha & -s\theta c\alpha s\phi + c\theta c\phi & -s\theta s\alpha c\phi - c\theta s\phi \\ s\alpha & c\alpha s\phi & c\alpha c\phi \end{bmatrix}_{t-1},$$

where c and s are the abbreviations for cos and sin, respectively, and T is the sampling period. The linear velocity vector $[v_{x_b} \quad v_{y_b} \quad v_{z_b}]^T$ is with respect to the body frame of the robot (x_b, y_b, z_b) defined in Section 3.1.

The RTI model extracted from the terrain map in Section 3.1 is treated as the measurement model. Therefore, the

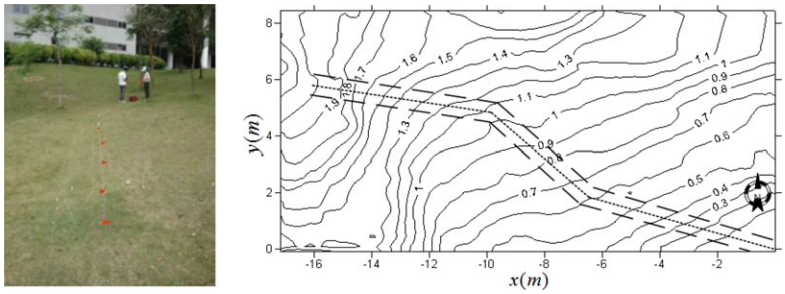

Figure 5. Picture of inclined terrains (left) and the topographical map of the navigation area (right)–Scenario 1.

measurement prediction can be described for each particle m as

$$\hat{z}_t^{[m]} = \begin{bmatrix} \hat{\theta}_t^{[m]} \\ \hat{\alpha}_t^{[m]} \\ \hat{\phi}_t^{[m]} \\ \hat{\text{dist}}_t^{[m]} \end{bmatrix} = \begin{bmatrix} \text{RTI model}_\theta(x_t^{[m]}, y_t^{[m]}, z_t^{[m]}) \\ \text{RTI model}_\alpha(x_t^{[m]}, y_t^{[m]}, z_t^{[m]}) \\ \text{RTI model}_\phi(x_t^{[m]}, y_t^{[m]}, z_t^{[m]}) \\ \text{dist}(p(x, y, z) - p(x_t^{[m]}, y_t^{[m]}, z_t^{[m]})) \end{bmatrix}, \tag{7}$$

where RTI model_θ, RTI model_α, and RTI model_ϕ consist of the RTI model extracted in the preceding section. $p(x_t^{[m]}, y_t^{[m]}, z_t^{[m]})$ represents the position of the particle m, and $p(x, y, z)$ represents the terrain point on the robot path closest to this particle that is gained from the map. $\hat{\text{dist}}_t^{[m]}$ is the distance between the particle m and the point $p(x, y, z)$.

To carry out the particle filter resample step, the weighting factor of each sample $w_t^{[m]}$ will be computed according to the sensor model,

$$z_t = [\theta_t, \alpha_t, \phi_t, \text{dist}_t], \tag{8}$$

where $[\theta_t, \alpha_t, \phi_t]^T$ is the measurement vector obtained from the onboard inertial sensors at the time interval T. The distance dist_t is not a real sensor measurement but a virtual measurement to keep all samples along the path at this moment. So dist_t is always zero (Mandel & Laue, 2010). The $w_t^{[m]}$ is computed by

$$w_t^{[m]} = |2\pi Q_t|^{-\frac{1}{2}} \exp\left\{-\frac{1}{2}\left(z_t - \hat{z}_t^{[m]}\right)^T\right\} Q_t^{-1}\left(z_t - \hat{z}_t^{[m]}\right). \tag{9}$$

The variation Q_t represents the uncertainty of the RTI model and the map inaccuracy.

4. EXPERIMENTAL RESULTS AND DISCUSSION

4.1. Methods and Procedures

The experiments were conducted on two platforms, a Summit XL robot (four-wheeled with suspension) and a Pioneer 3-DX robot (three-wheeled rigid). The NAV440 from Crossbow Technology® was used as the inertial measurement unit (IMU) that mounted on the top surface of the robot in order to measure the roll, pitch, yaw angles, and the angular velocities ω_{x_b}, ω_{y_b}, ω_{z_b}. The measurement accuracy is 0.5 degree in the roll and pitch directions and 1 degree in the yaw direction. The forward speed v_{x_b} with respect to the body frame was provided by the encoders of the robot. v_{y_b}, v_{z_b} are both zero with respect to the body frame with a no-slip assumption. Four outdoor scenarios have been selected in the area around Shenzhen University for experimental validation.

Table I. Experimental setups–Scenario 1.

Initial position errors (m)	Contour intervals (m)
(0.1,0.1,0.1);	0.05;
(0.2,0.2,0.2);	0.1;
(0.5,0.5,0.5)	0.2;
	0.3;
	0.4;
	0.5

Scenario 1: This scenario covers an approximate area of grassland that is 15 m × 10 m (see Figure 5). A group of experiments were conducted in Scenario 1 with different experimental setups using the Pioneer platform (see Table I) in order to evaluate how the initial conditions would affect the performance of the proposed technique. Three different initial estimations were used for extensive evaluation (see Table I). Different contour intervals of the topographical map were also plotted to evaluate the effect of the map accuracy on the robot performance (see Table I. To explore the bound of the proposed algorithm, contour intervals were established from 0.05 up to 0.5 m, which spans the range of the topographical maps plotted by motion capture and the commercial topographical maps (available at http://www.gzjtch.com/index.html, or http://www.bluewatersolutions.ca/lidar). At least three runs were conducted repeatedly for each experimental setup. The sampling period for all experiments was 0.1 s.

Scenario 2: This scenario covers an approximate area of soil of 15 m × 4 m. The Summit platform was used.

To evaluate how the surface roughness would affect the performance of the proposed technique, different sized stones were scattered to set up three surfaces with different roughness (see Figure 6). The point clouds map was obtained by a 3D laser scan system before the experiments only to evaluate the surface roughness. Taking advantage of the technique in Ye and Borenstein (2004), the point clouds map was divided into a series of terrain patches based on the size of the robot. Then a plane was fitted to every terrain patch using the least-squares error (LSE) approach, and the roughness of the terrain patch was indexed by σ, the residual of the fit between the point clouds data in the patch and the corresponding fitted plane. Therefore, the roughness of three terrain surfaces in Figure 6 was calculated as 0.38, 1.07, and 2.68 cm, respectively. According to Schuler, Lee, Kasilingam, and Nesti (2002), three categories were defined: smooth surface ($0 \leq \sigma < 0.4$ cm), intermediate rough surface ($0.4 \leq \sigma < 0.9$ cm), and rough surface ($\sigma \geq 0.9$ cm). Figure 6(a) shows the smooth surface, Figure 6(b) shows what could be treated as a lower bound of the rough surface, while Figure 6(c) shows what was considered to be a heavily rough surface.

An inertial sensor is the main sensor in the proposed technique. To characterize the effect of the sensor on the performance of the proposed method, a few different inertial sensors were simulated based on the sensor model [Eq. (10)], where w is the measured value, w_{true} is the true value, η is the angle random walk, and ε is the bias instability (Jerath & Brennan, 2011),

$$w = w_{\text{true}} + \eta + \varepsilon. \tag{10}$$

Two parameters are commonly used to adjust the performance of the inertial sensors, such as the angle random walk coefficient (RWC) and the bias instability coefficient (BIC) (Jerath & Brennan, 2011). To examine how the lower-performance sensors would degrade the proposed algorithm, the BIC started from 0.003deg/s (NAV440) up to 0.1 deg/s and the RWC started from 0.0075 deg $/\sqrt{\text{s}}$ (NAV440) up to 0.04 deg $/\sqrt{\text{s}}$.

Scenario 3: This scenario covers an approximate area of 60 m $\times$ 40 m with different types of rigid terrains, including downgrade and even sideways upgrade soils and upgrade and downgrade grasslands (see Figure 7). The entire traversed trip was 150 m long with a loop closure. The experiments conducted on the Pioneer platform in Scenario 3 were used to demonstrate that the proposed technique is applicable for longer trips with different types of terrains.

To generate a topographical map before all the experiments, a series of parallel lines, each spaced by 0.5 m on the terrain surface, were plotted to cover the whole navigation area. Then, the LED marker was moved along these lines to obtain the coordinate information of each line. These coordinates were used ultimately to obtain the topographical map (see Figure 5). Taking advantage of this method, the map resolution could be easily adjusted to evaluate the effects of the map's accuracy on the performance of the robot localization in the experiments.

Scenario 4: The area spans approximately 50 m $\times$ 80 m. The robot (Summit XL) traversed three loops with a total travel distance of 585 m (see Figure 12). Notice that in this outdoor environment, the robot will encounter both even and uneven terrains. So the experiments conducted in Scenario 4 are used to show how the proposed technique can be combined with the traditional method to identify the position of the robot in more general outdoor environments.

A 3D laser scan system (SICK LMS200+a turntable) was built on top of the mobile robot to achieve the traditional method when the robot traversed the even terrains in Scenario 4.

In such a setting, the continuous ground truth value was difficult to obtain online since the motion capture system could not cover the whole navigation area at one time. Hence a few discrete artificial markers were labeled along the real robot path during each experiment. The corresponding time interval was also recorded for each marker. Then

Figure 6. Three surfaces with different roughness–Scenario 2.

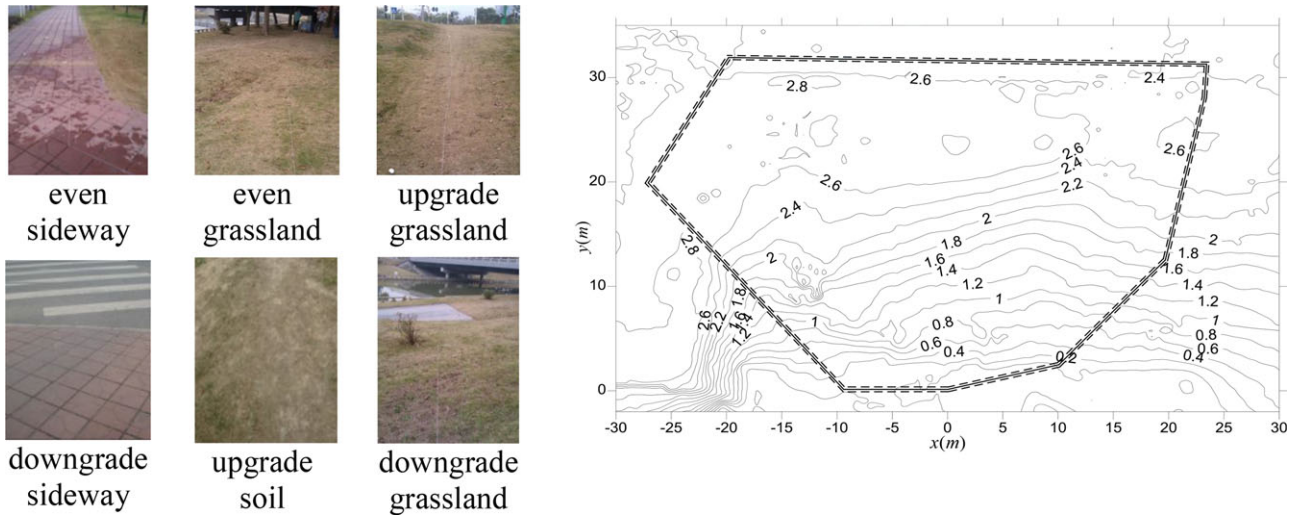

Figure 7. Pictures of the long trip with different types of terrains (left) and the topographical map of the navigation area (right)–Scenario 3.

the positions of those markers were measured individually by the motion capture system as the reference values after each experiment was done.

4.2. Results and Discussion

Scenario 1: The RTI model was extracted using the algorithm in Section 3.1. Based on this RTI model, the localization was achieved by applying the particle filter algorithm with 500 particles in Section 3.2. Eighteen discrete ground truth values were measured in each experimental trial.

The estimation of the robot position using the proposed technique (solid line) is compared with the dead-reckoning results (dashed-dotted line) and the reference positions (circle signs) in Figure 8 with the robot speed 0.05 m/s and the contour interval 0.05 m. According to Figure 8, the position estimation obtained using the proposed technique is much closer to the ground truth values in this type of outdoor scenario. To consider the ability to deal with the associated uncertainties, the localization performance using different filter algorithms, such as the extended Kalman filter (EKF) and the particle filter, has also been compared in Figure 8. Figure 8 indicates the position estimation based on the particle-filter-based TIL (solid line); our proposed method is much smoother than the one estimated by the EKF (dotted line).

To evaluate how the initial position error, ΔE, would affect the robot's performance, the 3D Euclidean distance between the estimated position and the reference position, Δd, is defined as the position estimation error, while the distance of the estimated position in the world coordinate is d. When the robot encountered the inclination variation of the terrain (i.e., crossing a contour line), the position estimation error was reduced quickly afterwards (e.g., after the distance of 3 m in Figure 9). According to Figure 9, The convergence of the position estimation errors is robust to large initial position errors up to 1.5 m.

It is necessary to analyze how the map resolution could affect the performance of the proposed method. Table II shows the average errors of position estimation under conditions of different contour intervals where the similarity between the RTI model and the measured attitude (defined in Section 3.1) is also checked to evaluate the uncertainties of the proposed measurement model. According to Table II, localization error is mostly increased monotonically as the contour interval increases, except for the case of a 0.2 m contour interval. The nonmonotonic effect at the contour interval of 0.2 m might be caused by the small error resulting from linear interpolation when the RTI model is generated (refer to Section 3.1). Nevertheless, the results do not show big differences among the contour intervals less than or equal to 0.3 m where the localization errors were all less than 0.1 m. The localization error is increased to 0.18 m with the contour interval 0.4 m because the similarity is downgraded to 66%, although the localization error is still much less than the dead-reckoning results (0.27 m). The proposed technique fails when the contour interval reaches 0.5 m, where the 43% similarity indicates very large uncertainty of the measurement model proposed in this paper. It is therefore concluded that lower map resolution would generally degrade the RTI model's accuracy, resulting in larger uncertainties of the measurement model. When these uncertainties are too large to be compensated by the particle filter, the proposed algorithm would be invalid.

Scenario 2: Table III shows the average estimation errors under conditions of different surface roughness with

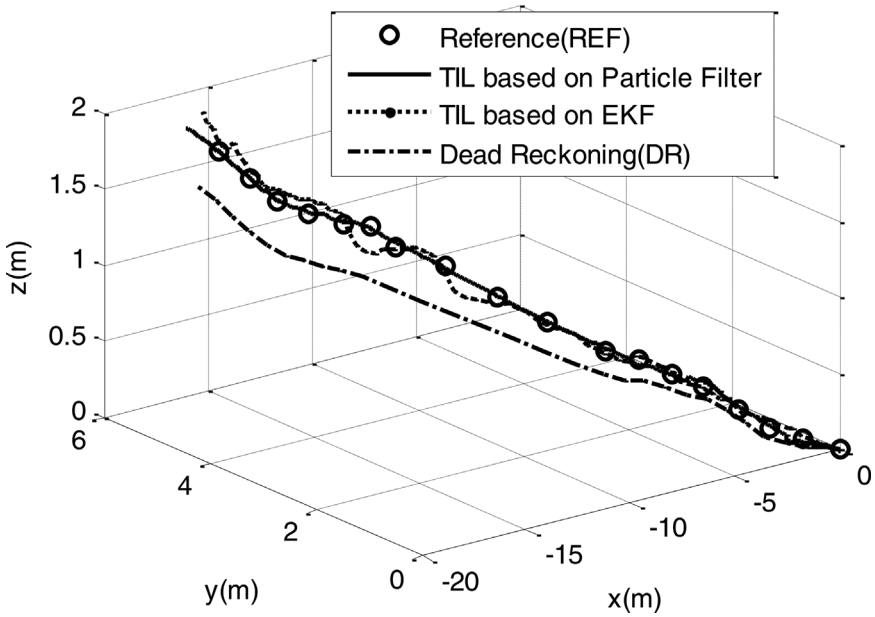

Figure 8. The position estimation comparison of the robot–Scenario 1. TIL denotes terrain-inclination localization. The solid line represents the proposed method in this paper while the dotted line represents the results when the particle filter is replaced by an EKF.

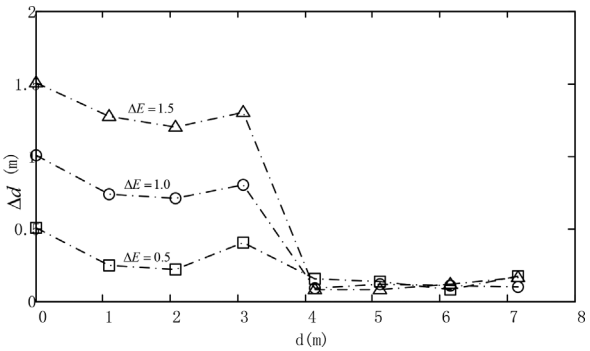

Figure 9. Position estimation errors at different initial errors, ΔE, along the route–Scenario 1.

Table II. Average errors of position estimation for different contour intervals–Scenario 1.

No.	Contour intervals (m)	Dead reckoning error (m)	Similarity (%)	Proposed method error (m)
1	0.05	0.27	0.76	0.072
2	0.1	0.27	0.75	0.077
3	0.2	0.27	0.78	0.069
4	0.3	0.27	0.72	0.081
5	0.4	0.27	0.66	0.18
6	0.5	0.27	0.43	0.47

the same contour interval 0.3 m. According to Table III, as the surface roughness increases, the localization errors using the proposed method and using the dead-reckoning method both increase. The variation of the similarity in Table III shows that the increasing surface roughness causes the uncertainties of the proposed measurement model to become larger. The localization performance becomes worse (up to 0.31 m) on the heavily rough surface. It is worth noting that the proposed method always has fewer errors than the dead-reckoning results on different roughness surfaces.

Figure 10 shows the average estimation errors of the proposed method using different simulated inertial sensors with the contour interval 0.3 m on the surface of Figure 6(a). The results indicate that the average estimated error increases as the angle random-walk coefficient (RWC) and the bias instability coefficient (BIC) increase. The localization error using the built-in inertial sensor of the hardware (NAV440) is 0.1 m, where (RWC, BIC) = (0.0075, 0.003). As (RWC, BIC) increased to the maximum values (0.04, 0.1) that are equivalent to a low-cost MEMS inertial sensor (Jerath & Brennan, 2011), the average estimation error increased to 0.15 m. Note that this was done on a relatively smooth surface. If the surface roughness varied along a long route, the performance would become worse. It is also expected that the tactical-grade inertial sensors could achieve better performance than the current MEMS sensor (NAV440). Hence a suitable inertial sensor should be

Table III. Average errors of position estimation for different surface roughness with the contour interval 0.3 m–Scenario 2.

No.	Surface type	Surface roughness (cm)	Dead reckoning error (m)	Similarity (%)	Proposed method error (m)
1	Smooth	0.38	0.21	0.73	0.10
2	Rough	1.07	0.39	0.69	0.18
3	Heavily Rough	2.68	0.43	0.63	0.31

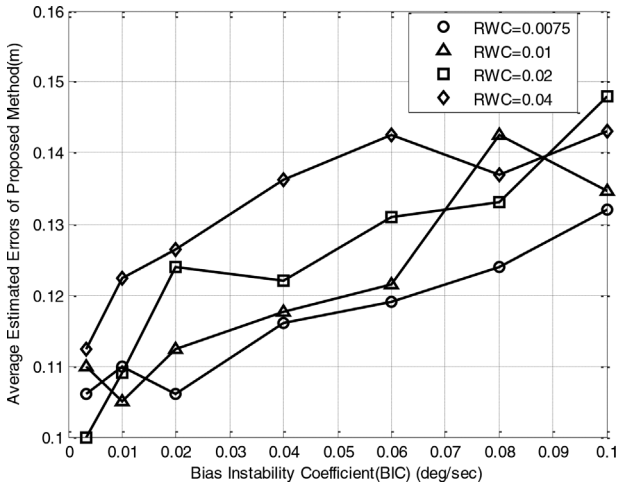

Figure 10. The average position estimation errors using different sensors parametrized by the angle random-walk coefficients (RWCs) and the bias instability coefficients (BICs)–Scenario 2.

selected for the proposed method depending on the requirement of localization performance.

Scenario 3: In this scenario, the RTI model was first extracted along the entire path on the topographical map according to the algorithm in Section 3.1. Forty-one discrete ground truth values were measured in this long trajectory.

Figure 11(a) shows a comparison of the position estimations using different methods. The estimation error at the destination point is 0.66 m with a 150 m travel distance using the proposed technique (solid line), while the estimation error is 5.48 m using the dead-reckoning method (dashed line). The robot positions obtained from only GPS are shown in Figure 11(b). According to Figure 11(b), the largest estimation error is more than 10 m based on GPS because the GPS signals were partially blocked by the surrounding trees and building. Therefore, the proposed terrain inclination localization technique can achieve satisfying performance when the GPS signals drift away.

Scenario 4: In this scenario, the robot traversed three loops. When the robot moved on uneven terrain, the proposed terrain inclination technique was applied to estimate the position of the robot. When the robot moved on even terrain, a fast iterative closest point (ICP) algorithm with point reduction and cached kd-tree (Nüchter, Lingemann, Hertzberg, & Surmann, 2007) was then applied to align the overlapped laser scan maps to update the position of the robot. Figure 12(a) shows the position estimation using terrain-inclination localization on uneven terrain (from P_1 to P_2) and the fast ICP on even terrain (from P_2 to P_1). According to Figure 12(a), the proposed technique can be combined with the fast ICP to identify the position of the robot in more general outdoor environments . The robot positions obtained from only GPS are shown in Figure 12(b).

Figure 13 depicts the position errors in three directions based on a combination of our proposed method and the fast ICP. According to Figure 13, our proposed method can quickly decrease the position errors, even though the fast ICP algorithm applied during the latter half of the previous loop does not provide good initial results. The maximum position error in three directions stays within 0.5 m when the robot moves on uneven terrain. Moreover, the estimation error does not accumulate as the robot continues to move during three loops.

It is therefore concluded that the proposed terrain-inclination-localization algorithms can efficiently achieve localization on 3D inclined terrain only when they are combined with the onboard inertial sensors when the GPS signals are inaccurate or lost for a long period of time.

5. CONCLUSIONS

This paper introduces a particle filter terrain-inclination-based 3D localization technique for a mobile robot operating on outdoor inclined terrains. Different factors such as map resolution, terrain surface roughness, and sensor accuracy were examined in the experiments to evaluate how the localization performance has been influenced. Experimental results validate the proposed technique and illustrate that the proposed technique has the capability to achieve localization with only onboard inertial sensors when GPS signals are blocked. It is concluded that the proposed method could form the basis of a stand-alone or complementary

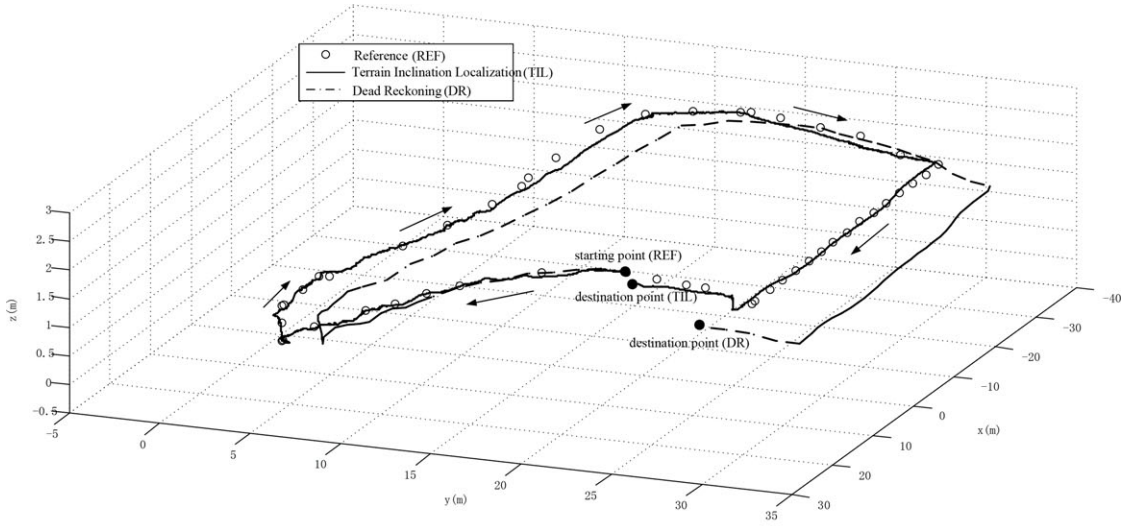

(a) The robot position estimated by our proposed method.

(b) The estimated path from GPS (red line) and the reference path (black circle).

Figure 11. The performance results for Scenario 3 with different types of terrains, where the robot traversed a loop with a length of 150 m–Scenario 3.

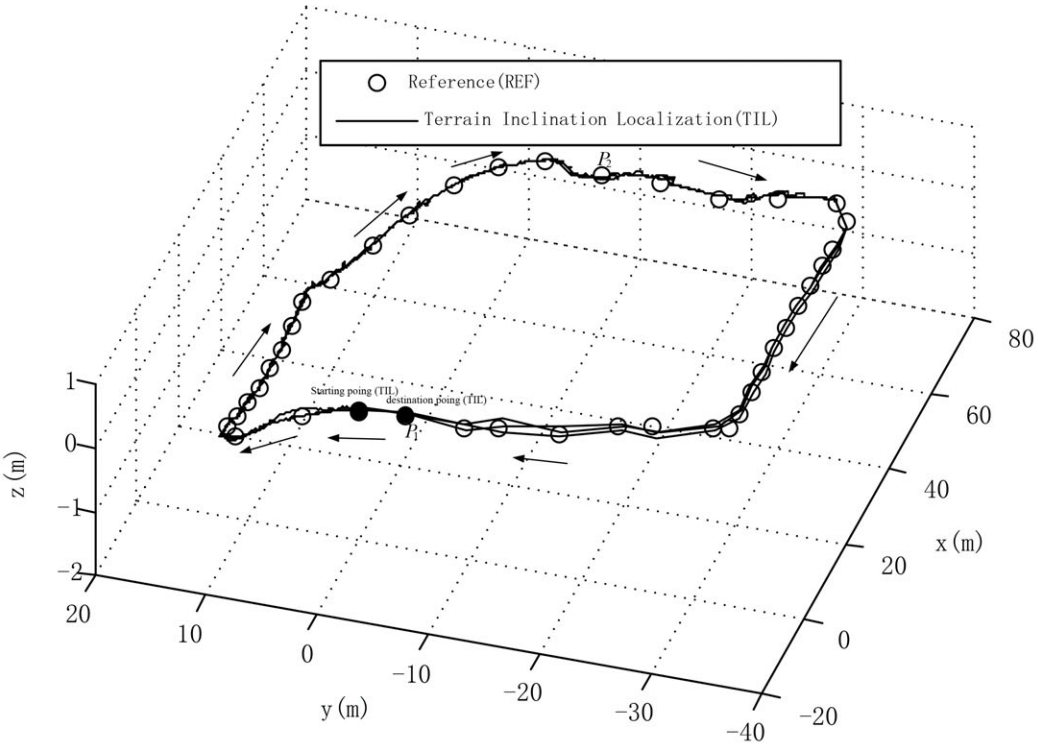

(a) The robot position estimated by our proposed method.

(b) The estimated path from GPS (red line) and the reference path (black circle).

Figure 12. The performance results for Scenario 4 with even and uneven terrains, where the robot traversed three loops with an overall length of 585 m.

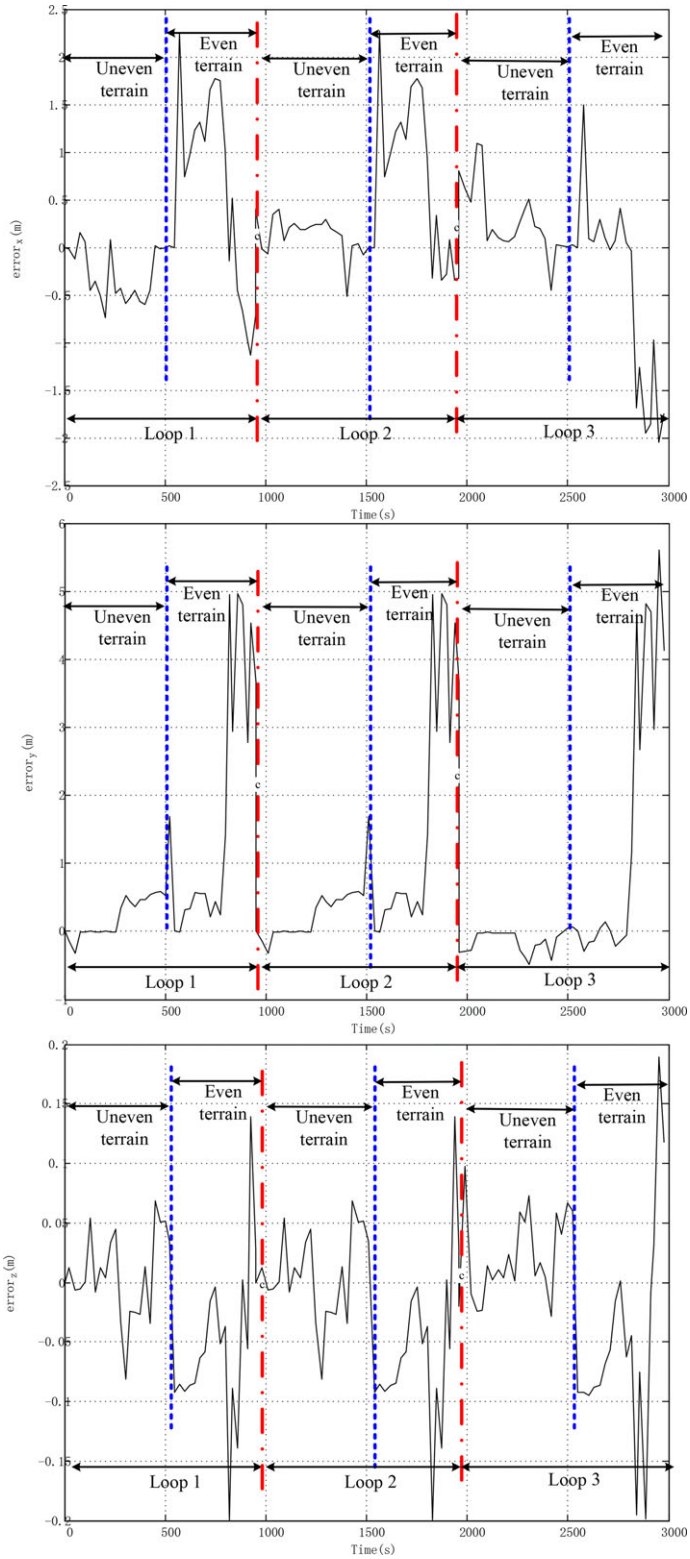

Figure 13. The position estimation errors of the robot using the proposed technique–Scenario 4.

localization method. Future work will focus mainly on accommodating more terrain features.

ACKNOWLEDGMENTS

This research is currently supported by the NSF of China under NSFC Grant No. 60905052. The thoughtful suggestions from Professor Mark Bodson and Professor Sandy Meek (University of Utah) made at the beginning of this work are appreciated.

REFERENCES

Barfoot, T. D. (2005). Online visual motion estimation using FastSLAM with sift features. In Proceedings of the IEEE/RSJ International Conference on Intelligent Robots and Systems (IROS), Edmonton, Canada.

Blaer, P., & Allen, P. (2002). Topological mobile robot localization using fast vision techniques. In Proceedings of the 2002 ICRA. IEEE International Conference on Robotics and Automation, Washington, D.C.

Bluewater (2010). LiDAR. Retrieved January 10, 2013, from http://www.bluewatersolutions.ca/lidar.

Borenstein, J., Everett, H. R., & Feng, L. (1996). Where am I? Sensors and methods for mobile robot positioning. University of Michigan, Ann Arbor, MI.

Bonnifait, P., Bouron, P., Crubille, P., & Meizel, D. (2001). Data fusion of four ABS sensors and GPS for an enhanced localization of car-like vehicles. In Proceedings of 2001 ICRA. IEEE International Conference on Robotics and Automation, Seoul, South Korea.

Bouvet, D., & Garcia, G. (2000). Civil-engineering articulated vehicle localization: Solutions to deal with GPS masking phases. In Proceedings of 2000 ICRA. IEEE International Conference on Robotics and Automation, San Francisco, CA.

Brenneke, C., Wulf, O., & Wagner, B. (2003). Using 3D laser range data for SLAM in outdoor environments. In Proceedings of the 2003 IEEE/RSJ International Conference on Intelligent Robots and Systems, Las Vegas, NV.

Brooks, C. A., & Iagnemma, K. (2005). Vibration-based terrain classification for planetary exploration rovers. IEEE Transactions on Robotics, 21, 1185–1191.

Burschka, D., & Hager, G. D. (2004). V-GPS(SLAM): Vision-based inertial system for mobile robots. In Proceedings of the 2004 IEEE International Conference on Robotics and Automation, New Orleans, LA.

Cancilliere, F. M. (1994). Advanced UUV technology. In Proceedings of OCEANS'94, Brest, France.

Chand, A., & Yuta, S. (2010). Road crossing landmarks detection by outdoor mobile robots. Robotics and Mechatronics, 22, 708–717.

Chekhlov, D., Pupilli, M., Mayol, & Calway, A. (2007). Robust real-time visual SLAM using scale prediction and exemplar based feature description. In Proceedings of the IEEE Conference on Computer Vision and Pattern Recognition, Minneapolis, MN.

Chen, H., Li, X., & Ding, W. (2007). Twelve kinds of gridding methods of Surfer 8.0 in isoline drawing. Chinese Journal of Engineering Geophysics, 4, 52–57.

Choset, H., & Nagatani, K. (2001). Topological simultaneous localization and mapping (SLAM): Toward exact localization without explicit localization. IEEE Transactions on Robotics and Automation, 17, 125–137.

Cumani, A., Denasi, S., Guiducci, A., & Quaglia, G. (2003). Integrating monocular vision and odometry for SLAM. WSEAS Transactions on Computers, 3, 625–630.

Dellaert, F., Fox, D., Burgard, W., & Thrun, S. (1999). Monte Carlo localization for mobile robots. In Proceedings of the 1999 IEEE International Conference on Robotics and Automation, Detroit, MI.

Diosi, A., & Kleeman, L. (2004). Advanced sonar and laser range finder fusion for simultaneous localization and mapping. In Proceedings of the 2004 IEEE/RSJ International Conference on Intelligent Robots and Systems (IROS), Sendai, Japan.

Erico, G. (2011). How Google's self-driving car works. IEEE Spectrum, 18.

Fairfield, N., Kantor, G., & Wettergreen, D. (2006). Real-time SLAM with octree evidence grids for exploration in underwater tunnels. Journal of Field Robotics, 23, 3–21.

Goulden, T. (2009). Prediction of error due to terrain slope in LiDAR observations. Department of Geodesy and Geomatics Engineering Technical Report, No. 265, University of New Brunswick, Fredericton, New Brunswick, Canada.

Hygounenc, E., Jung, I. K., Soueres, P., & Lacroix, S. (2004). The autonomous blimp project of laas-cnrs: Achievements in flight control and terrain mapping. International Journal of Robotics Research, 23(4–5), 473–511.

Iagnemma, K., & Dubowsky, S. (2004). Mobile robots in rough terrain: Estimation, motion planning, and control with application to planetary rovers. Springer.

Jerath, K., & Brennan, S. N. (2011). GPS-free terrain-based vehicle tracking performance as a function of inertial sensor characteristics. In Proceedings of ASME Dynamic Systems and Control Conference, New York.

JianTong Survey (2012). Products and services. Retrieved January 10, 2013, from http://www.gzjtch.com/sitecn/chcp/index.html

Kawewong, A., Tongprasit, N., Tangruamsub, S., & Hasegawa, O. (2010). Online and incremental appearance-based SLAM in highly dynamic environments. International Journal of Robotics Research, 30(1), 33–33.

Kummerle, R., Triebel, R., Pfaff, P., & Burgard, W. (2008). Monte Carlo localization in outdoor terrains using multilevel surface maps. Journal of Field Robotics, 25, 346–359.

Laanaya, H., Martin, A., Khenchaf, A., & Aboutajdine, D. (2005). Feature selection using genetic algorithm for sonar images classification with support vector machines. European Conference on Propagation and Systems, Brest, France.

Lamon, P., & Siegwart, R. (2007). 3D position tracking in challenging terrain. International Journal of Robotics Research, 26(2), 167–186.

Madhavan, R., & Durrant-Whyte, H. F. (2004). Natural landmark-based autonomous vehicle navigation. Robotics and Autonomous Systems, 46, 79–95.

Manandhar, D., & Shibasaki, R. (2001). Feature extraction from range data. In Proceedings of the 2001 22nd Asian Conference on Remote Sensing (ACRS), Singapore.

Mandel, C., & Laue, T. (2010). Particle filter-based position estimation in road networks using digital elevation models. In Proceedings of the IEEE/RSJ International Conference on Intelligent Robots and Systems, Taipei, Taiwan.

Martin, M. C., & Moravec, H. (1996). Robot evidence grids. Technical Report CMU-RI-TR-96-06, Robotics Institute, Carnegie Mellon University, Pittsburgh, PA.

Minor, M. A., Albiston, B., & Schwensen, C. (2006). Simplified motion control of a two axle compliant framed wheeled mobile robot. IEEE Transactions on Robotics, 22, 491–506.

Nagatani, K., Ishida, H., Yamanaka, S., & Tanaka, Y. (2003). Three-dimensional localization and mapping for mobile robot in disaster environments. In Proceedings of the 2003 IEEE/RSJ International Conference on Intelligent Robots and Systems, Las Vegas, NV.

Nasrallah, D. S., Angeles, J., & Michalska, H. (2005). Modeling of an anti-tilting outdoor mobile robot. In Proceedings of the DETC2005: ASME International Design Engineering Technical Conferences and Computers and Information in Engineering Conference, Long Beach, CA.

Nüchter, A., Lingemann, K., Hertzberg, J., & Surmann, H. (2007). 6D SLAM-3D mapping outdoor environments. Journal of Field Robotics, 24(8/9), 669–722.

Pfaff, P., Triebel, R., & Burgard, W. (2007). An efficient extension to elevation maps for outdoor terrain mapping and loop closing. International Journal of Robotics Research, 26(2), 217–230.

Roberts, J. M., Corke, P. I., Cunningham, J., & Durrant-Whyte, H. (1998). Automation of underground LHD & truck haulage. In Proceedings of the 1998 AusIMM Annual Conference on Mining Cycle, Mount Isa.

Schuler, D. L., Lee, J. S., Kasilingam, D., & Nesti, G. (2002). Surface roughness and slope measurements using polarimetric SAR data. Transactions on Geoscience and Remote Sensing, 40, 687–698.

Surmann, H., Nuchter, A., & Hertzberg, J. (2003). An autonomous mobile robot with a 3D laser range finder for 3D exploration and digitalization of indoor environments. Robotics and Autonomous Systems, 45, 181–198.

Talukder, A., Manduchi, R., Castano, R., Owens, K., Matthies, L., Castano, A., & Hogg, R. (2002). Autonomous terrain characterization and modelling for dynamic control of unmanned vehicles. In Proceedings of the 2002 IEEE/RSJ International Conference on Intelligent Robots and Systems, Lausanne, Switzerland.

Theunissen, E., Koeners, G. J. M., Rademaker, R. M., Jinkins, R. D., & Etherington, T. J. (2005). Terrain following and terrain avoidance with synthetic vision. In Proceedings of the 24th Digital Avionics Systems Conference, Washington, D.C.

Thrun, S., Burgard, W., & Fox, D. (2005). Probabilistic robotics. Cambridge, MA: MIT Press.

Tongprasit, N., Kawewong, A., & Hasegawa, O. (2011). PIRF-Nav 2: Speeded-up online and incremental appearance-based SLAM in an indoor environment. In Proceedings of the 2011 IEEE Workshop on Applications of Computer Vision, Washington, D.C.

Triebel, R., Pfaff, P., & Burgard, W. (2006). Multi-level surface maps for outdoor terrain mapping and loop closing. In Proceedings of the International Conference on Intelligent Robots and Systems (IROS), Beijing, China.

Weisbin, C. R., Rodriguez, G., Schenker, P. S., Das, H., Hayati, S. A., Baumgartner, E. T., Maimone, M., Nesnas, I. A., & Volpe, R. A. (1999). Autonomous rover technology for Mars sample return. In Proceedings of iSAIRAS'99. Fifth International Symposium on Artificial Intelligence, Robotics and Automation in Space, Noordwijk, The Netherlands.

Ye, C., & Borenstein, J. (2004). A method for mobile robot navigation on rough terrain. In Proceedings of the IEEE International Conference on Robotics and Automation, New Orleans, LA.

Zelenka, R. E., Clark, R. F., Zirkler, A., Saari, R., & Bragan, R. G. (1996). Development and flight test of terrain-referenced guidance with ladar forward sensor. Journal of Guidance, Control, and Dynamics, 19, 823–828.

Zhu, X., Kim, Y., Merrell, R., & Minor, M. A. (2007). Cooperative motion control and sensing architecture in compliant framed modular mobile robots. IEEE Transactions on Robotics, 23, 1095–1101.

Zhu, X., Minor, M. A., & Park, S. (2006). Distributed robust control of compliant framed wheeled modular mobile robots. ASME Journal of Dynamic Systems, Measurement, and Control, 128, 489–498.

Zhu, X., Qiu, C, & Minor, M. A. (2013). Terrain inclination aided three-dimensional localization and mapping for an outdoor mobile robot. International Journal of Advanced Robotic Systems, 10, 76.

Zhuang, Y., Wang, W., Wang, K., & Xu, X. D. (2005). Mobile robot indoor simultaneous localization and mapping using laser range finder and monocular vision. Zidonghua Xuebao/Acta Automatica Sinica, 31, 925–933.